

# Non-equilibrium quantum dots: transport

M A Reed, J N Randall and J H Luscombe

Central Research Laboratories, Texas Instruments Incorporated, Dallas, TX 75265, USA

Received 10 March 1990, in final form 19 March 1990

**Abstract.** The electronic transport through three-dimensionally confined semiconductor 'quantum dots' is investigated and analyzed. The spectrum corresponds to resonant tunneling from laterally confined emitter contact subbands through the discrete three-dimensionally confined quantum dot states. Momentum non-conservation is observed in these structures.

## 1. Introduction

Carrier confinement to reduced dimensions has led to numerous important developments in basic semiconductor physics and device technology. Advances in microfabrication technology [1–3] now allow one to impose quantum confinement in more than one dimension, typically done by constricting or confining in lateral dimensions an existing 2D carrier system. The realization of semiconductor quantum wires [4, 5] and the creation of 'electron waveguides' [6] has allowed the investigation of well-defined lateral subbands in a semiconductor (not metallic) host. These structures are excellent laboratories to study fundamentals of electronic transport [7–10]. Unfortunately, the relevant transport in these structures can only be done near equilibrium (i.e. low voltages, with low temperatures) and thus these measurements do not shed light on more common non-equilibrium semiconductor situations.

Recently, three-dimensionally confined 'quantum dots' have been realized [11]. These structures are analogous to semiconductor atoms, with energy levels tunable by the confining potentials. However, quantum dot structures pose an experimental paradox. Establishing transport through the single electronic states of a quantum dot implies the states cannot be totally isolated; i.e. the confining potential must be slightly leaky, and thus the states are quasi-bound. Additionally, contact to higher-dimensional carrier reservoirs is non-trivial from an experimental and analysis viewpoint.

We have adopted a configuration where the quasi-bound momentum component (and thus the resultant transport direction) is epitaxially defined in the form of a resonant tunneling structure, with additional confinement fabrication-imposed. This configuration is distinct in that it is through, not along, the epitaxial interface. Because of this, the behavior of a system operated far from equilibrium can be examined. We present here a study of resonant tunneling through various quantum

dot systems, and the bandstructure modeling necessary to understand the experimental electronic transport spectra.

## 2. Fabrication and transport

Our approach to producing quantum dot nanostructures suitable for electronic transport studies is to laterally confine resonant tunneling heterostructures. This approach embeds a quasi-bound quantum dot between two quantum wire contacts.

AuGe/Ni/Au ohmic metallization dots (single or multiple dot regions) are defined by electron-beam lithography on the surface of the grown resonant tunneling structure. Creation of dots less than 300 Å is possible, though we will show that the appropriate range for the typical epitaxial structure and process used is in the range 1000–2500 Å in diameter. A bilayer polymethylmethacrylate (PMMA) resist and lift-off method is used. The metal dot ohmic contact serves as a self-aligned etch mask for highly anisotropic reactive ion etching (RIE) using  $\text{BCl}_3$  as an etch gas. The resonant tunneling structure is etched through to the  $n^+$ -GaAs bottom contact, defining columns in the epitaxial structure. A SEM of a collection of these etched structures is seen in figure 1.

To make contact with the tops of the columns, a planarizing and insulating polyimide is spun on the sample, then etched back by  $\text{O}_2$  RIE to expose the metal contacts on the top of the columns. A gold contact pad is then evaporated over the top of the column(s). The bottom conductive substrate provides electrical continuity. Multiple columns can be connected in parallel for diagnostic purposes; however, it should be stressed that all data discussed hereupon is for a single isolated column.

Figure 2 shows the current–voltage–temperature characteristics of a quantum dot resonant tunneling

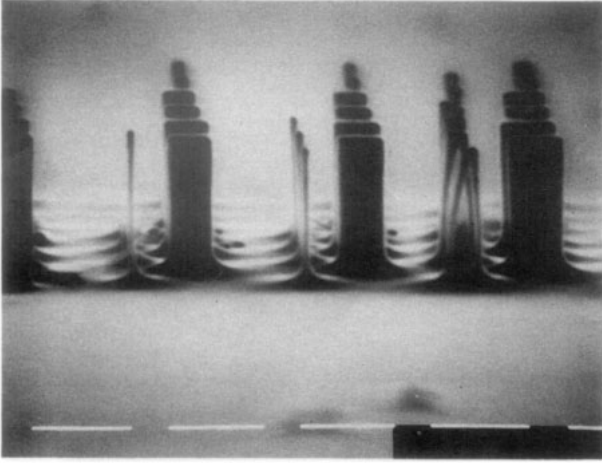


**Figure 1.** SEM of an array of anisotropically etched columns containing a quantum dot. The horizontal marker is  $0.5 \mu\text{m}$ ; the diameter of the smallest columns is approximately  $200 \text{ \AA}$ . The dark region on top of the column is the electron-beam defined ohmic contact/etch mask.

structure. The structure lithographically is  $1000 \text{ \AA}$  in diameter and epitaxially is a  $n^+$ -GaAs contact/AlGaAs barrier/InGaAs quantum well structure. At high temperature, the characteristic negative differential resistance of a double barrier resonant tunneling structure is observed. As the temperature is lowered, two effects occur. First, the overall impedance increases. Second, a series of peaks appears above and below the main negative differential resistance (NDR) peak. In the range of device bias  $0.75$ – $0.90 \text{ V}$ , the peaks appear equally spaced with a splitting of approximately  $50 \text{ mV}$ . Another peak, presumably due to the ground state of the harmonic oscillator potential, occurs  $80 \text{ mV}$  below the equally spaced series.

The existence of the fine structure in the tunneling characteristics of this, and other, laterally confined reso-

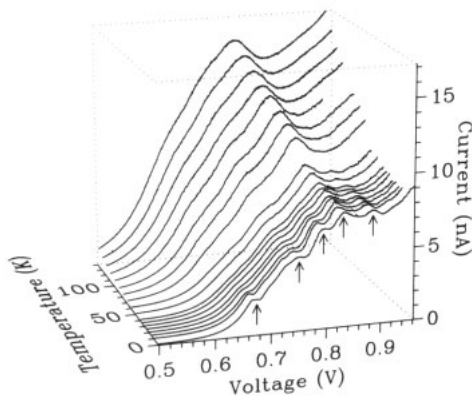


**Figure 2.** Current–voltage–temperature characteristics of a single-quantum-dot nanostructure, indicating resonant tunneling through the discrete states of the quantum dot. The structure lithographically is  $1000 \text{ \AA}$  in diameter and epitaxially is a  $n^+$ -GaAs contact/AlGaAs barrier/InGaAs quantum well structure. The arrows indicate voltage peak positions of the discrete state tunneling for the  $T = 1.0 \text{ K}$  curve.

nant tunneling structures indicates the formation of laterally confined electronic states. However, a full indexing of the spectrum is needed to verify that the structure in the electrical characteristics is the discrete levels. To do this, a full 3D screening model of the quantum dot system is necessary.

### 3. 3D quantum dot modeling

We have modeled the full screening potential of the quantum dot system taking into account the effects of lateral confinement [12]. Cylindrical symmetry is assumed. The model self-consistently obtains the electrostatic potential in a zero-current theory from Poisson's equation utilizing a Thomas–Fermi approximation for the electron density. The solution of the electrostatic problem then provides the potential responsible for lateral quantization of electron states, which we obtain from the radial Schrödinger equation in cylindrical coordinates. The radial bound states in the contacts provide the minima of the emitter and collector subbands. Likewise the discrete quantum well levels, which in the absence of lateral confinement would otherwise form a two-dimensional subband, are obtained from a solution of the radial Schrödinger equation. We shall first consider only the zero-angular-momentum ( $l = 0$ ) states.

The boundary conditions necessary for a solution to the quantum dot screening potential are considerably more complicated than for the 1D problem. At the center of the post ( $r = 0$ ), a simple Neumann condition of zero electric field was imposed. More involved is the question of the proper Dirichlet boundary condition to employ for the contact regions of this laterally confined system. It is not enough to set the boundary potential in the degenerately doped contacts to achieve charge neutrality, as one would have in a one-dimensional simulation or for bulk systems where surface effects are irrelevant. The restricted lateral extent of the quantum dot system, with the Fermi level pinning at the exposed outer lateral surface, implies a solution to the Poisson equation in the radial direction which is not a simple constant. Thus, to obtain a boundary condition in the contact regions for the full quantum dot system, we first do a 1D self-consistent calculation for the radial direction, using the Laplacian for cylindrical coordinates. The boundary conditions for this calculation are again a zero-field condition at the origin and another Neumann condition at the external radius set by an amount of surface charge necessary to support the value of the Fermi level pinning. To match up with the calculation for the full problem, it is assumed that there is negligible variation of the potential in the vertical direction in the vicinity of where the contact boundary conditions are to be imposed. The calculation is quite sensitive to the boundary condition specified at the outer lateral surface. We have employed a Neumann condition where the slope is determined by the surface charge. We allow this quantity to vary in the vertical direction. Our model assumes, to a first approxi-

mation, a constant density of surface states per unit area, independent of the material composition or doping level. We assume however that these states are occupied according to a Fermi–Dirac distribution, with the value of the Fermi level pinning acting as a local chemical potential. This rudimentary model of the surface charge distribution effectively pins the computed potential at the external lateral surface to the desired Fermi level pinning value. The calculation itself adjusts the occupation of surface states to self-consistently achieve a constant surface potential in the vertical direction (for zero bias) independent of material or doping level variations.

The equilibrium solution to the 3D screening problem using the quantum dot epitaxial structure and the measured physical radius of the column is displayed in figure 3. The electron potential energy surface is plotted as a function of radius ( $R$ ) and epitaxial ( $z$ ) dimensions. The radial extent is 0–500 Å and the vertical length is approximately 2000 Å, centered about the double barriers. The energy scale is defined relative to the Fermi energy, thus the potential at the external radius equals 0.7 V. The contours in the contact regions are the occupied laterally defined subbands that lie below the Fermi level. For this specific case of radial dimension and contact doping level, three contact subbands are occupied. The subband energies are determined by solving the radial Schrödinger equation. For clarity, the quantum dot energy levels are not drawn in figure 3.

It has been suggested [13] that the observed quantum dot spectrum can be explained as resonances when the quantum dot states are biased through the emitter subband states with increasing device bias. To determine if this mechanism quantitatively explains the spectrum, we solve the 3D self-consistent screening quantum dot model at applied bias, to determine the variation of the emitter and quantum dot energy levels with applied voltage. The bias voltage positions of the quantum dot

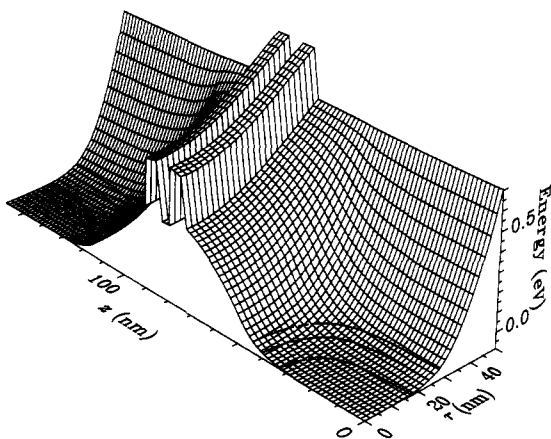


**Figure 3.** Self-consistent 3D band diagram of the previously detailed single quantum dot structure, at equilibrium. The electron potential energy surface is plotted as a function of radius ( $R$ ) and epitaxial ( $z$ ) dimensions. The contours in the contact regions are the occupied laterally-defined subbands. For clarity, the quantum dot energy levels are not drawn.

resonances are then determined by generating a family of surfaces similar to figure 3 and determining the eigenvalues.

Figure 4 shows the crossings of the emitter subband levels ( $n'$ ) with the quantum dot levels ( $n$ ) as a function of applied bias. The parameters of the quantum dot model were the same as those detailed previously [12]. Figure 5 shows the crossings of the emitter subbands with the quantum dot states, transposed onto the 1.0 K current–voltage characteristic of the quantum dot, with a spacer width of 177 Å and with the initial and final state index numbers labeled  $n'-n$ . There is general agreement between the experimental and predicted peak voltage positions, especially the anomalously large splitting of the first resonance. This can be seen as a consequence of the subband-level crossing mechanism, when more than one lateral subband is below the Fermi level. The experimental peaks differ from the predicted peak positions by at most 15 mV, which corresponds to approximately 5 meV in energy. This is in good agreement, considering the approximations of zero-current, homogeneous dopant distributions, and perfect radial symmetry. It should also be noted that the experimental measurement is current, which implies that an integration over the density of emitter states should be done for a strict comparison. It is possible that peaks may be shifted in voltage or even washed out when this is correctly done; however, the qualitative and quantitative agreement of the peak positions suggests this may not be a significant effect.

Note that the predicted  $3'-3$  transition appears to be absent in the spectrum, except for a very weak structure at 0.92–0.93 V. However, this is not unexpected since the collector barrier becomes sufficiently low such that this state becomes virtual at resonant bias. This has an important implication—verification that the observed resonances are due to states localized in the quantum dot and not due to the density of states in the collector contact.

The preceding calculations are for angular momenta ( $l$ ) equal to zero. Higher angular momentum states can be

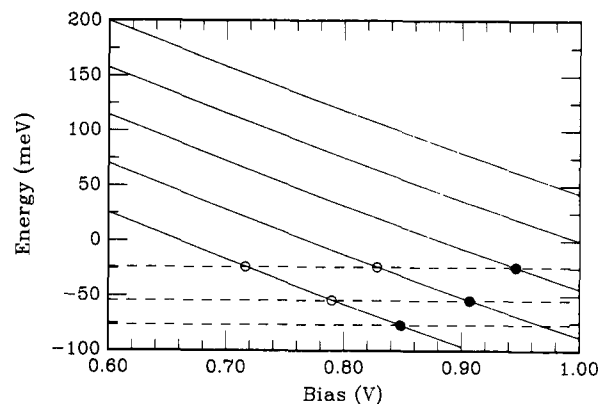


**Figure 4.** Emitter subband levels ( $n'$ ) and the quantum dot levels ( $n$ ) as a function of applied bias. The circles denote the crossings; solid for momentum-conserving ( $n = n'$ ) transitions and open for momentum-non-conserving ( $n \neq n'$ ) transitions.

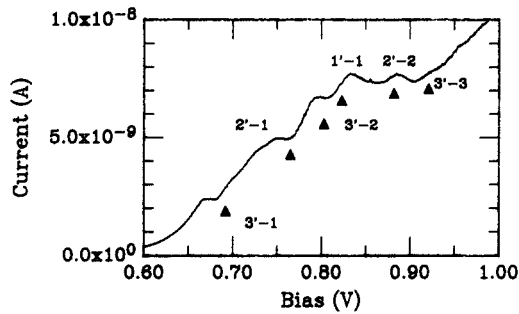


**Figure 5.** Current-voltage characteristic at  $T = 1.0$  K of the previously detailed single quantum dot structure, with predicted resonant peak positions and initial and final state index numbers ( $n'-n$ ).

calculated, and effectively split the spectra into  $l \times$  (number of  $n'-n$  crossings). Such extra structure does not seem evident in our experimental data, though sharper peak shapes are very desirable. Preliminary magnetic field studies up to 9.0 T show no obvious Zeeman split discrete level peaks, which should be observable by 2.0 T if higher angular momenta states were occupied. This implies not only a  $\Delta l = 0$  selection rule, but a restriction to  $l = 0$  as well.

As a result of indexing the transitions, we can determine selection rules for the transitions. The observation of the momentum-non-conserving transitions ( $n' \neq n$ ) show that  $n$  is *not* a conserved quantity in this quantum dot system.

This is because naïvely assumed momentum conservation assumes translational symmetry, which has been broken here. Also note that the topography of the electron energy surface implies a  $\Delta l = 0$  selection rule. It should be emphasized that selection rules derive from the symmetries of the system, and that the breakdown of intuitive selection rules for these nanostructured semiconductor atomic analogies arise from the difference between the fabrication-imposed potential and other assumed potentials.

#### 4. Conclusions

Quantum dot structures provide a unique laboratory for the exploration of quantum transport through nanostructured semiconductors. The 'atomic states' can be

varied with structural variables, allowing for the exploration of the fundamentals of quantum-confined electronic states, transitions, and selection rules involving those states.

#### Acknowledgments

We wish to thank R T Bate for constant encouragement and support, William R Frensley, Rajni J Aggarwal, Richard J Matyi, Tom M Moore, and Anna E Wetsel for their contributions and R K Aldert, E D Pijan, D A Schultz, P F Stickney, and J R Thomason for technical assistance. This work was sponsored by the Office of Naval Research, the Army Research Office, and the Air Force Wright Avionics Laboratory.

#### References

- [1] Broer A N, Molzen W W, Cuomo J J and Wittels N D 1976 *Appl. Phys. Lett.* **29** 596
- [2] Howard R E, Liao P F, Skocpol W J, Jackel L D and Craighead H G 1983 *Science* **221** 117
- [3] Craighead H G 1984 *J. Appl. Phys.* **55** 4430
- [4] van Houten H, van Wees B J, Heijman M G J and Andre J P 1986 *Appl. Phys. Lett.* **49** 1781
- [5] Berggren K F, Thornton T J, Newson D J and Pepper M 1986 *Phys. Rev. Lett.* **57** 1769
- [6] Timp G, Chang A M, Mankiewich P, Behringer R, Cunningham J E, Chang T Y and Howard R E 1987 *Phys. Rev. Lett.* **59** 732
- [7] Landauer R 1957 *IBM J. Res. Dev.* **1** 223
- [8] Büttiker M 1986 *Phys. Rev. Lett.* **57** 1761
- [9] van Wees B J, van Houten H, Beenakker C W J, Williamson J G, Kouwenhoven L P, van der Marel D and Foxon C T 1988 *Phys. Rev. Lett.* **60** 848
- [10] Wharam D A, Thornton T J, Newbury R, Pepper M, Ahmed H, Frost J E F, Hasko D G, Peacock D C, Ritchie D A and Jones G A C 1988 *J. Phys. C: Solid State Phys.* L209
- [11] Reed M A, Randall J N, Aggarwal R J, Matyi R J, Moore T M and Wetsel A E 1988 *Phys. Rev. Lett.* **60** 535
- [12] Reed M A, Randall J N, Luscombe J H, Frensley W R, Aggarwal R J, Matyi R J, Moore T M and Wetsel A E 1989 *Quantum Dot Resonant Tunnelling Spectroscopy (Festkörperprobleme/Advances in Solid State Physics)* vol 29, ed U Rössler (Braunschweig: Vieweg)
- [13] Bryant G W 1989 *Phys. Rev. B* **39** 3145